https://doi.org/10.5194/egusphere-2026-4480
Preprint. Discussion started: 4 September 2026

Holocene hydroclimatic reorganization and prehistoric settlement response in the East Asian summer monsoon transition zone

Xiaoshuang Sun[a], Rui Han[a], Mengyi Yang[a], Jinliang Liu[b], Tianlong Yan[c], Xin Mao[d, *], Can Zhang[e, **]

a School of civil engineering and geomatics, Shandong University of Technology, Zibo 255000, China

b School of Environmental Sciences, Nanjing Xiaozhuang University, Nanjing 211171, China

c School of Geography, Liaoning Normal University, Dalian 116021, China

d Institute of Hydrogeology and Environmental Geology, Chinese Academy of Geological Sciences, Shijiazhuang, 050061, China

e State Key Laboratory of Lake and Watershed Science for Water Security, Nanjing Institute of Geography and Limnology, Chinese Academy of Sciences, Nanjing 211135, China

Corresponding author: czhang@niglas.ac.cn (C. Zhang); maoxin.iheg@cnu.edu.cn (X. Mao)

https://doi.org/10.5194/egusphere-2026-4480
Preprint. Discussion started: 4 September 2026

Abstract: Holocene hydroclimatic changes in the East Asian monsoon region were spatially heterogeneous, but their timing and driving mechanisms within the monsoon transition zone remain insufficiently constrained. Here, we present a multi-proxy biomarker record from Nansi Lake, eastern China, to reconstruct Holocene hydroclimatic variability in this sensitive monsoon transition belt. The record indicates relatively dry conditions during the early Holocene, a pronounced humid interval during the middle Holocene, and generally drier but more variable conditions during the late Holocene. This pattern is broadly consistent with the middle-Holocene moisture maximum recorded in northern China, but contrasts with central-sector records characterized by wetter early and late Holocene conditions and drier mid-Holocene. Beyond this latitudinal contrast, proxy records across the monsoon transition zone reveal a longitudinal hydroclimatic gradient, with peak Holocene humidity generally delayed from west to east. This eastward delay may have been modulated by changes in El Niño activity and regional topographic effects on monsoon moisture transport. Furthermore, comparison with archaeological site distributions suggests that this hydroclimatic reorganization was accompanied by an eastward shift in prehistoric settlement density within the transition zone. These findings highlight the spatial complexity of Holocene hydroclimatic change in monsoon transition regions and provide a long-term perspective on landscape–human interactions under changing moisture regimes.

Keywords: East Asian monsoon; Holocene hydroclimate; Longitudinal difference; El Niño activity and topographic; Historical human settlement.

https://doi.org/10.5194/egusphere-2026-4480
Preprint. Discussion started: 4 September 2026

1. Introduction

The East Asian summer monsoon (EASM) is a major component of the global monsoon system, and variations in its precipitation has exerted long-term influence on ecosystem structure, hydrological processes, and water-resource availability across the East Asian summer monsoon (EASM; An et al., 2000). The Holocene, following the last deglaciation, provides a usef ul temporal framework for examining the evolution of the EASM because it was marked by substantial hydroclimatic variability (Chen et al., 2015). Although numerous speleothem, lacustrine, and peat records have been widely used to reconstruct Holocene EASM precipitation variability, the spatial patterning and dominant controls of these changes remain unresolved. Speleothem oxygen-isotope records commonly pointed to relatively coherent, orbitally paced changes in monsoon circulation (Li et al., 2026). By contrast, quantitative reconstructions from lake and peat archives reveal pronounced regional hydroclimatic differences, indicating that monsoon intensity and regional precipitation were not linked through a simple one-to-one relationship (An et al., 2000; Liu et al., 2021; Li et al., 2023; Rao et al., 2016).

A central issue of this debate is the spatiotemporal structure of Holocene precipitation across the EASM domain. The classical interpretation emphasizes an asynchronous Holocene optimum across East Asia (An et al., 2000), whereas more recent syntheses suggest that at least two distinct precipitation modes can be recognized within the EAM region (Chen et al., 2015; Liu et al., 2021; Li et al., 2023; Rao et al., 2016). One is a dipole pattern inferred from multiple proxy records (Chen et al., 2015; Liu et al., 2021), and the other is a tripole pattern, first identified from modern instrumental precipitation patterns and later supported by paleoclimate evidence (Rao et al., 2016; Li et al., 2023). For example, multiple quantitative reconstructions from northern China generally indicate relatively humid conditions during the middle Holocene (Chen et al., 2015; Sun and Feng, 2013; Xu et al., 2010). In contrast, records from the middle and lower reaches of the Yangtze River commonly suggest a drier middle Holocene, with wetter conditions during the early and late Holocene (Li et al., 2025; Liu et al., 2019; Liu et al., 2021; Zhu et al., 2017). Recent regional syntheses and model simulations further indicate that annual and summer precipitation across the EAM region were generally enhanced during the early to middle Holocene, although long-term trajectories differed markedly between northern and southern China (Li et al., 2024; Li et al., 2026). Together, these results suggest that Holocene precipitation patterns were shaped by the combined effects of orbital forcing, residual ice sheets, and ocean–atmosphere interactions (Li et al., 2024; Li et al., 2026).

The East Asian monsoon transitional zone (east of 105°E, near 35°N) between northern and central China (lower Yangtze River region) and broadly coincides with the modern humid-semi-humid climatic boundary, making it a key area for evaluating contrasting interpretations of Holocene precipitation patterns. Recent pollen-based quantitative reconstructions from the Central Plains at central transitional zone show that Holocene precipitation in this region followed neither the northern pattern nor that of the middle and lower Yangtze patterns, but instead displayed marked transitional and stage-dependent characteristics. These records highlight the possible influence of ENSO variability and the associated meridional displacement of the Western Pacific Subtropical High on regional precipitation redistribution (Li et al., 2023; Liu et al., 2025). Compared with the Central Plains, Holocene precipitation reconstructions from southern Shandong remain space. This area occupies a key transitional position between North China, the Central Plains, and the Jianghuai region. This geographic position makes it particularly sensitive to shifts in the monsoonal rain belt.

Here, we use sedimentary records from Nansi Lake in southern Shandong to reconstruct Holocene precipitation evolution in this key transitional region. The objectives are to: (1) identify the timing of humid and dry phases in the southern Shandong during the Holocene and assess their correspondence with records from northern China and the middle–lower Yangtze region; (2) characterize the variability of Holocene hydrological records within the transitional zone; and (3) examine the mechanisms responsible for Holocene hydrological evolution.

https://doi.org/10.5194/egusphere-2026-4480
Preprint. Discussion started: 4 September 2026

2. Materials and methods

2.1 Study site

Nansi Lake (34°27′–35°20′N, 116°34′–117°21′E; ~35 m a.s.l.; Fig. 1a, b), situated in southwestern Shandong Province, China, is a large shallow freshwater lake system (Shen et al., 2000). The lake complex is composed of four hydrologically connected sub-lakes, namely Nanyang, Dushan, Zhaoyang, and Weishan, and stretches for about 126 km in a north–south direction. It has a total area of approximately 1,266 km^2 and a mean water depth of about 1.5 m (Zhang et al., 1999). Lake hydrology is mainly sustained by regional precipitation and local runoff, and the drainage ultimately connects to the Huai River system (Shen et al., 2000). The lake is surrounded by a flat alluvial plain, where the natural vegetation is dominated by grasses, herbs, shrubs such as Artemisia and Chenopodiaceae, and various aquatic plants. According to meteorological observations from the Jining station for 1981–2010 (Fig. 1c), mean annual precipitation is about 670 mm, with nearly 85% falling between May and October. Mean annual temperature is approximately 15 °C, and monthly mean temperatures range from about 26.3 °C in July to about 4 °C in January.

2.2 Sample collection and chronology

In 2022, a 2.45-m sediment core was collected from the central basin of northern Nansi Lake (35°04′51.4938″N, 116°44′54.7197″E) at a water depth of ~2.79 m using a piston corer mounted on a UWITEC platform. After recovery, the core was described lithologically and then subsampled at 1-cm resolution. All samples were refrigerated at 4 °C prior to subsequent analyses. Nansi Lake shot core were analyzed for the ^{210}Pb and ^{137}Cs activities using a gamma spectrometer (Fig. 2d). The age-depth relationship of short core with dating uncertainty was established using the constant rate of supply (CRS) model (Appleby and Oldfield, 1978). In addition, five organic clay samples from the deeper part of the core were selected for accelerator mass spectrometry (AMS) radiocarbon dating at Beta Analytic (Fig. 2c). Radiocarbon ages were converted to calibrated calendar ages before present (BP; 0 BP = 1950 CE) using the IntCal20

https://doi.org/10.5194/egusphere-2026-4480
Preprint. Discussion started: 4 September 2026

calibration curve (Reimer et al., 2020). The age–depth relationship was constructed with Bacon, a Bayesian age-modelling approach that incorporates both calibrated ages and stratigraphic depth information. The resulting chronology suggests that the sediment sequence covers roughly the last 9 ka (Fig. 2c), with sediment accumulation rates varying through time. The uppermost interval shows relatively rapid accumulation, probably related to recent changes in hydrological conditions and sedimentary processes.

2.3 Lipid extraction and alkane analysis

A total of 116 sediment samples from the Nansi Lake long core were analysed for lipid extraction following the below chemical pretreatment. Freeze-dried samples (3 g) were ultrasonically extracted four times using dichloromethane:methanol (9:1, *v*/v). After concentrating with N2, the extracted total lipids were saponified using 6% KOH in methanol solution for 12 h. The supernatant was collected after adding NaCl and n-hexane and centrifuging. Finally, the neutral supernatant containing *n*-alkanes was extracted through silica gel column.

The *n*-alkanes were measured by an Agilent 7890 Gas Chromatography (GC) device equipped with a flame ionized detector and a split injector, HP1-ms GC column (60 m*0.32 mm, 0.50 µm film thickness). The detailed oven procedure is to hold for 1 min at 40 °C, heat to150 °C at a rate10 °C/min, then rise to 310 °C at a rate of 6 °C/min, and finally hold for 60 min at 310 °C (Sun et al., 2023).

Multiple parameters, including the P_{aq} (Ficken et al., 2000), alkane C_{23}/C_{31} (Ficken et al., 2000), LPTP (Chu et al., 2014) were as following:

$$P_{aq} = (nC_{23} + nC_{25}) / (nC_{23} + nC_{25} + nC_{29} + nC_{31}).$$

$$LPTP = (nC_{17} + nC_{19} + nC_{21} + nC_{23} + nC_{25})/(nC_{27} + nC_{29} + nC_{31} + nC_{33})$$

Where C_i is the n-alkane concentration of *i* number.

2.4 Spatiotemporal kernel density analysis of archaeological sites

Archaeological site data were extracted from Hosner et al. (2016) and grouped into six 1000-year intervals from 8000 to 2000 cal yr BP. Kernel density estimation (KDE) was performed in ArcGIS using the Kernel Density tool to convert the point distribution

https://doi.org/10.5194/egusphere-2026-4480
Preprint. Discussion started: 4 September 2026

of archaeological sites into continuous density surfaces for each time interval. The same search radius, cell size, and spatial extent were applied to all KDE maps to ensure comparability among time slices. Following previous spatiotemporal archaeological studies, KDE values were interpreted as relative archaeological site density rather than absolute population size (Zhang et al., 2022). The resulting maps were used to identify temporal changes in high-density settlement areas and to compare their spatial shifts with regional hydroclimatic variations.

3 Results and Discussion

3.1 Paleoclimatic implication of n-alkanes proxies

The alkanes in lake sediments are a mixture of allochthonous sources from the catchment and autochthonous source produced within the lake (Castaneda and Schouten, 2011; Garcin et al., 2014). In general, long-chains (C_{27}-C_{33}) n-alkanes are mainly produced by terrestrial plants, and mid-chain (C_{23}-C_{25}) n-alkanes originating from aquatic plants, while short-chain (C_{17}-C_{21}) n-alkanes predominantly originate from algae and bacterial (Aichner et al., 2010; Ficken et al., 2000; Lin et al., 2024; Nichols et al., 2009; Zhang et al., 2019). Sedimentary n-alkanes from Nansi Lake are characterized by a clear mid-chain dominance, with C_{25} as the main peak and C_{23} and C_{27} as secondary peaks, whereas long-chain homologues (e.g., C_{29}, C_{31}, and C_{33}) are comparatively less abundant (Fig. 3a-d). This distribution is commonly interpreted as indicating predominantly in-lake aquatic organic matter input, with only limited contribution from terrestrial higher plants. The broadly consistent n-alkane patterns across different intervals further indicate that the dominant organic matter source remained largely stable through time (Fig. 3a-d). This interpretation is supported by generally high P_{aq} values (Fig. 3e), which are typically associated with enhanced submerged/floating macrophyte input and shallow lacustrine settings (Ficken et al., 2000; Sun et al., 2023; Zhang et al., 2019). The alkane C_{23}/C_{31} ratio and LPTP show similar variations (Fig. 3f, g), further supporting this inference. High C_{23}/C_{31} values, together with elevated LPTP, indicate a stronger contribution from aquatic organic

https://doi.org/10.5194/egusphere-2026-4480
Preprint. Discussion started: 4 September 2026

matter, whereas lower values suggest increased terrestrial input (Chu et al., 2014; Inglis et al., 2015). In the Nansi Lake profile, both proxies remain relatively high during the mid-Holocene (Fig. 3e-f), implying expanded aquatic vegetation and greater in-lake organic matter production, but decline and become more variable during the late Holocene, pointing to a stronger terrestrial influence and less stable organic matter sources. Because light availability and water depth strongly constrain submerged macrophyte habitats in shallow lakes (Lacoul and Freedman, 2006), an expanded lake area would have provided more favorable habitat for aquatic vegetation. We therefore infer that precipitation-driven lake water depth changes regulated aquatic vegetation in Lake Nansi and, in turn, controlled sedimentary P_{aq}. In this setting, P_{aq} provides a useful indicator of effective moisture variability.

3.2 Latitudinal variation patterns in the East Asian monsoon region

Our hydroclimate reconstruction at Nansi Lake from the eastern of the transition zone indicates generally dry conditions during the early Holocene, followed by a gradual increase in precipitation and the development of relatively humid conditions during the mid-Holocene, particularly between 6000 and 2500 cal yr BP (Fig. 4d). This pattern is broadly consistent with previous evidence from the Nansi Lake region. For example, optically stimulated luminescence dating indicates that the lake area expanded during ~5000–3000 cal yr BP, followed by a general contraction (Fig. 5e; Tian et al., 2025). Similarly, pollen and grain-size records from Judian Lake indicate that between 6810 and 3100 cal yr BP, increased abundances of *Quercus* and *Ulmus*, together with strengthened hydrodynamic conditions and enhanced sediment transport capacity, reflected a generally humid climate (Zou et al., 2020). At a latitudinal scale, comparison of the Nansi Lake record with other regional archives reveals pronounced spatial heterogeneity in Holocene hydroclimate across EAM region. In northern China, records from Daihai Lake (Fig. 4a; Xu et al., 2010), Qigai Nuur Lake (Fig. 4b; Sun and Feng, 2013), and Gonghai Lake (Fig. 4c; Chen et al., 2015), many records indicate increase precipitation during the middle Holocene (8000 to 3000 cal yr BP), followed by a shift toward drier after 3000 cal yr BP. By contrast, records from central China, for example

https://doi.org/10.5194/egusphere-2026-4480
Preprint. Discussion started: 4 September 2026

Heshang Cave (Fig. 4f; Zhu et al., 2017), Dajiuhu peat (Fig. 4g; Liu et al., 2019), Jianghan Plain (Fig. 4h; Li et al, 2025), and Nanyi Lake (Fig. 4 I; Liu et al., 2021), generally point to reduced moisture during the middle Holocene (8000-3000 cal yr BP). Although differing in Some details, the Nansi Lake record is more closely aligned with that of northern China than with those from central China, as both indicate a broadly humid phase during the middle Holocene.

3.3 Longitudinal patterns of hydroclimatic variability across the transition zone

A comparison with other longitudinal records across transition belt further indicates that Holocene hydroclimatic evolution was not spatially uniform. For example, pollen-based precipitation reconstructions from the central of the transition zone, including records from the Mianchi Basin (Li et al., 2023) and Xingyang Basin (Liu et al., 2025), show several moisture shifts through the Holocene rather than a single sustained trend (Fig. 5c). Their relatively wet phases are mainly centered at 8000–7200 cal yr BP and 4000–2500 cal yr BP, with the driest conditions occurring between 7200 and 4000 yr BP. By contrast, a 10Be-based precipitation reconstruction from the Baoji Loess at west of the transition zone indicates maximum precipitation before 5500 cal yr BP, followed by a rapidly decline (Fig. 5c; Beck et al., 2018). Similarly, precipitation records inferred from magnetic susceptibility in the Pingyang and Dadiwan Loess suggest a wet interval during 8000-5000 cal yr BP (Fig. 5c; Gao et al., 2019; Liu et al., 2020). The asynchronous timing of maximum Holocene humidity across the transition zone is further supported by paleoflood records (Fig. 5a, d; Gao et al., 2025; Xiao et al., 2026). Paleofloods records from the western and central parts of the transition zone show event clusters at 8500–7000 and 4500–2000 cal yr BP (Fig. 5a), broadly matching the staged hydroclimatic evolution inferred for this sector (Fig. 5b, c). By contrast, paleoflood records from the eastern part of transition zone indicate a markedly increase in flood frequency during ~5000–2000 yr BP (Fig.5d), broadly corresponding to the main humid phase for this sector (Fig. 5e). Taken together, these comparisons indicate that the timing of maximum Holocene humidity varied across the transition belt, but appears to have been delayed from west to east, with the peak humid occurring earlier

https://doi.org/10.5194/egusphere-2026-4480
Preprint. Discussion started: 4 September 2026

in the western part and later in the eastern region.

Variations in El Niño activity may have contributed to the west-to-east delay in the timing of maximum Holocene humidity across the transition region. Before ~6500 cal yr BP, El Niño activity was relatively strong (Koutavas and Joanides, 2012), precipitation appears to have been enhanced in the western part, whereas the eastern sector remained comparatively dry (Fig. 5c, e). During ~6500–3000 cal yr BP, as El Niño activity weakened (Koutavas and Joanides, 2012), the zone of maximum moisture shifted gradually eastward, while the western region experienced a drying trend (Fig. 5c, e). This interpretation is supported by modern observational data, which show that the contrasting west-east precipitation anomalies within the transition belt during the 1951-1978 and 1979-1992 were closely associated with changes in El Niño activity (Fig. 6; Ding et al., 2008). During the 1951 to 1978, relatively weak El Niño activity, was accompanied by increase precipitation in the eastern sector and decline in the west part (Fig. 6a). Conversely, during 1979 to 1992, when El Niño activity was strengthened, precipitation increased in the western part but decreased in the eastern sector (Fig. 6b). The central part of the transition was characterized by a bimodal humid pattern during the middle Holocene (Fig. 6).

Topographic modulation may have been further amplified these spatial differences. The eastern sector is dominated by relatively open terrain, whereas the central and western parts are more strongly affected by mountain blocking and orographic uplift (Fig. 1b). During the early mid-Holocene, a stronger EASM drove the monsoon rain belt further north (Chen et al., 2015). Moisture may therefore have crossed the open plains rapidly, limiting persistence rainfall in the eastern sector, whereas orographic uplift enhanced precipitation along the western mountains front. During the late mid-Holocene, monsoon weakening and a more restricted rain-belt migration may have increased rainfall residences time over the eastern sector but reduced precipitation penetration across western mountains. This mechanism is consistent with reconstructed precipitation changes in the Qinling Mountain (Zhang et al., 2025) and with modern climatological evidence showing that the Qinling Mountains can reorganize low-level moisture transport, enhance convective instability, and promote upward motion along the mountain front (He et al., 2008; Li et al., 2021). Together, El Niño activity and topographic modulation likely contributed to the asynchronous timing of Holocene humidity maxima within the transition belt.

3.3 Influence of longitudinal hydroclimatic variability on prehistoric human settlement patterns

To explore the possible link between settlement activity and regional hydroclimatic change, we compared reconstructed moisture records with spatiotemporal kernel density of archaeological sites across hydroclimatic transition zone. The KDE results show clear changes in the location of high-density settlement areas from 8000-2000 cal yr BP (Fig. 7), proving a spatial perspective for evaluating the relationship between hydroclimatic reorganization and prehistoric human occupation.

In the western sector, moisture records suggest relatively humid conditions during ca. 8000–5000 cal yr BP (Fig. 5c). During this period, high-density archaeological cluster were mainly distributed in the western parts of the transition zone (Fig. 7a-c), broadly corresponding to the Laoguantai, Yangshao cultural phases (Hosner et al., 2016). Many settlements in this region were located along river valleys, loess tablelands and terrace margins, where access to water, cultivable land, and relatively stable landforms favored occupation and farming (Hosner et al., 2016; Zhang et al., 2024). The temporal agreement between wetter conditions and increased settlement density suggests that improved moisture availability may have supported rain-fed millet agriculture and settlement expansion, consistent with archaeobotanical evidence from northern China and the Guanzhong–Loess Plateau region (Li et al., 2009; He et al., 2022; Leipe et al., 2019). At the same time, the Dadiwan sequence shows that settlement development was not controlled by climate alone, but was closely related to cultural continuity, subsistence innovation, and regional interaction (Pei et al., 2026). After 5000 cal yr BP, moisture conditions weakened in the western sector, and the KDE pattern shows that high-density settlement areas became less concentrated there (Fig. 7d-f), possibly reflecting reduced environmental support for stable rain-fed settlement

https://doi.org/10.5194/egusphere-2026-4480
Preprint. Discussion started: 4 September 2026

together with changes in cultural organization and settlement strategy (Zhang et al., 2024).

In the central sector, archaeological site density increased during the late mid-Holocene, especially during the Yangshao and Longshan occupations during the late mid-Holocene (Fig. 7c-d; Hosner et al., 2016). Regional hydroclimatic records also indicate enhanced moisture availability or stronger hydrological activity during this interval (Fig. 5b). Pollen-based reconstructions from the Mianchi and Xingyang basins show pronounced Holocene hydroclimatic fluctuations, suggesting that the Central Plains was a sensitive part of the East Asian summer monsoon transition zone rather than an area with a simple wet–dry trajectory (Li et al., 2023; Liu et al., 2025). In the Luoyang Basin, phases of increased precipitation and wetland expansion at 7400–6550, 5650–5050, and 4350–3950 yr BP were associated with agricultural intensification and settlement growth, especially during the late Yangshao and late Longshan periods (Chen and Li, 2025). Improved water supply and the availability of alluvial land may have favored settlement aggregation in basin environments. At the same time, paleoflood evidence around 4200 cal yr BP indicates that stronger hydrological activity also brought higher flood risk to riverine and lowland settings (Zhang and Xia, 2011; Gao et al., 2025). Thus, in the central sector, increased moisture may have favored settlement aggregation in basin environments, but intensified hydrological activity also introduced flood-related risks, making the relationship between hydroclimate and settlement development more complex.

In the eastern sector, the Nansi Lake record and regional lacustrine evidence point to enhanced hydrological conditions from 6000 to 2500 cal yr BP (Fig. 5e). This interval overlaps with the Dawenkou, Longshan, Yueshi, and Shang–Zhou periods represented in the archaeological record (Fig. 7a; Hosner et al., 2016). The KDE maps show that high-density settlement clusters became increasingly prominent in the eastern part of the transition zone during the late mid-Holocene (Fig. 7d-e). Unlike the western sectors, this area was more closely tied to river–lake systems, lowland wetlands, and floodplain environments. During the Dawenkou and Longshan periods, humid conditions, wetland resources, and rice or mixed farming may have provided a favorable basis for settlement

https://doi.org/10.5194/egusphere-2026-4480
Preprint. Discussion started: 4 September 2026

growth (Jin and Wang, 2010; Ding et al., 2011; Yang et al., 2016). In the Yishu River Basin, warm and wet conditions during the early and middle Longshan period were associated with developed paddy agriculture and abundant archaeological sites, suggesting that hydroclimatic suitability and agricultural productivity were closely linked to settlement expansion (Gao et al., 2007). However, cooling and hydrological instability around ca. 4200 cal yr BP may have affected rice agriculture and contributed to the Longshan–Yueshi transition (Gao et al., 2007; Ding et al., 2011). The later increase during the Zhou period may reflect a recovery or reorganization of settlement systems under new forms of land use and water management.

Taken together, the comparison between hydroclimatic records and KDE-based archaeological site density suggests that settlement change across the transition zone were not spatially static. High-density settlement areas were more prominent in the western and central sector during the early mid-Holocene, whereas they became increasingly concentrated in the eastern sector during the late mid-Holocene. This spatial shift broadly corresponds to the eastward reorganization of favorable hydrological conditions shown by regional moisture and lacustrine records. Thus, hydroclimatic change provided an important environmental background for the eastward reorganization of prehistoric settlement density, although the final settlement pattern was also shaped by cultural and social factors (Chen and Li, 2025; Dong et al., 2019).

4. Conclusion

This study reconstructed Holocene hydroclimatic changes in the Nansi Lake region using sedimentary *n*-alkane proxies. The dominance of mid-chain and the variations in P_{aq}, C_{23}/C_{31}, and LPTP indicate that aquatic plants were the main source of sedimentary organic matter. The reconstructed records suggest the region experienced relatively high lake levels and enhanced effective moisture during the mid-Holocene. Since the late Holocene, declining and more variable proxy values suggest a shift toward less stable hydrological conditions and increased terrestrial input.

The hydroclimatic evolution of Nansi Lake was characterized by relatively a

https://doi.org/10.5194/egusphere-2026-4480
Preprint. Discussion started: 4 September 2026

pronounced humid phase at approximately 6000–2500 cal yr BP, and a general weakening of moisture conditions thereafter. This pattern is broadly consistent with records from northern China at latitudinal scale, but differs from the mid-Holocene dry pattern documented in the central China. Comparisons with other records from the transition belt further reveal marked longitudinal delay in the maximum humidity. The west-to-east contrast of precipitation indicate that Holocene precipitation patterns were jointly influenced by El Niño activity and region topographic modulation.

In addition, archaeological site distributions in the transitional zone further indicate that human occupation center broadly tracked the Holocene eastward migration of precipitation, with early to mid-Holocene settlement concentrated in the western sector and later activity increasing in the central and eastern part. This connection suggests that shifts in precipitation reshaped agricultural suitability and settlement stability, thereby promoting a gradual eastward shift in the center of human activity within the EAM transitional zone.

Acknowledgments

This study is supported by the National Key Research and Development Program of China (2023YFF0807201), National Natural Science Foundation of China (42371167, 42407598), Shandong Provincial Natural Science Foundation (ZR2025MS634).

Author Contributions

Xiaoshuang Sun and Can Zhang conceive and designed the study. Mengyi Yang Jinliang Liu, Tianlong Yan, Xin Mao collected and analyzed the samples. Xiaoshuang Sun, Rui Han, Can Zhang perform the data analysis and visualization. Xiaoshuang Sun, Can Zhang write the original draft. All authors reviewed and approved the final manuscript.

Conflict of Interest

The authors declare no conflicts of interest relevant to this study.

https://doi.org/10.5194/egusphere-2026-4480
Preprint. Discussion started: 4 September 2026

Data Availability

The n-alkane data generated in this study is freely available in the Figshare repository: https://doi.org/10.6084/m9.figshare.32731563.

References

Aichner, B., Herzschuh, U., Wilkes, H., 2010. Influence of aquatic macrophytes on the stable carbon isotopic signatures of sedimentary organic matter in lakes on the Tibetan Plateau. Org. Geochem. 41, 706–718.

An, Z.S., Porter, S.C., Kutzbach, J.E., Wu, X.H., Wang, S.M., Liu, X.D., Li, X.Q., Zhou, W. J., 2000. Asynchronous Holocene optimum of the east asian monsoon. Quat. Sci. Rev. 19, 743–762. https://doi.org/10.1016/S0277-3791(99)00031-1.

Appleby, P.G., Oldfield, F., 1978. The calculation of lead-210 dates assuming a constant rate of supply of unsupported 210Pb to the sediment. CATENA 5, 1–8. https://doi.org/10.1016/S0341-8162(78)80002-2.

Beck, J.W., Zhou, W.J., Li, Cheng., et al. 2018. A 550,000-year record of East Asian monsoon rainfall from 10Be in loess. Science, 360, 877–881.

Castaneda, I.S., Schouten, S., 2011. A review of molecular organic proxies for ~ examining modern and ancient lacustrine environments. Quat. Sci. Rev. 30, 2851e2891

Chen, F., Xu, Q., Chen, J., Birks, H.J., Liu, J., Zhang, S., Jin, L., An, C., Telford, R.J., Cao, X., Wang, Z., Zhang, X., Selvaraj, K., Lu, H., Li, Y., Zheng, Z., Wang, H., Zhou, A., Dong, G., Zhang, J., Huang, X., Bloemendal, J., Rao, Z., 2015. East Asian summer monsoon precipitation variability since the last deglaciation. Sci. Rep. 5, 11186.

Chen, L., Li, K.F. 2025. Mid-Holocene hydroclimatic changes drove Neolithic agricultural development in the Luoyang Basin of the Central Plains, China. Catena, 258, 109241.

Chu, G., Sun, Q., Xie, M., Lin, Y., Shang, W., Zhu, Q., Shan, Y., Xu, D., Rioual, P., Wang, L., Liu, J., 2014. Holocene cyclic climatic variations and the role of the

https://doi.org/10.5194/egusphere-2026-4480
Preprint. Discussion started: 4 September 2026

Pacific Ocean as recorded in varved sediments from northeastern China. Quat. Sci. Rev. 102,85–95.

Cui, J.X., Sun, Z.Y., Burr, G.S., et al. 2019. The great cultural divergence and environmental background of Northern Shaanxi and its adjacent regions during the late Neolithic. Archaeological Research in Asia, 20, 100164.

Ding, M., Peng, S.Z., Pang, J.L., et al. 2011. Holocene Environmental Change and Its Impacts on Cultural Development in the Central Region of Shandong Province. Chinese Journal of Soil Science, 42, 6. (In Chinese with English abstract).

Ding, Y., Wang, Z., Sun, Y., 2008. Inter-decadal variation of the summer precipitation in East China and its association with decreasing Asian summer monsoon. Part I: observed evidences. Int. J. Climatol. 28, 1139–1161.

Dong, G.H., Li, R., Lu， M.X., 2019. Evolution of human–environmental interactions in China from the Late Paleolithic to the Bronze Age. Progress in Physical Geography, 1-18.

Ficken, K.J., Li, B., Swain, D.L., Eglinton, G., 2000. An *n*-alkane proxy for the sedimentary inputs of submerged/floating freshwater aquatic macrophytes. Org.Geochem. 31, 745–749

Gao, F.Y., Jia, J., Xia, D.S., Lu, C.C., Lu, H., Wang, Y.J., Liu, H., Ma, Y.P., Li, K.M., 2019. Asynchronous Holocene Climate Optimum across mid-latitude Asia. Paleogeogr. Paleoclimatol. Paleoecol. 518, 206–214.

Gao, H.Z., Cheng, Zhu, C., Xu, WF. 2007. Environmental change and cultural response around 4200 cal. yr BP in the Yishu River Basin, Shandong. 285-292. DOI: 10.1007/s11442-007-0285-5.

Gao, W.H., Li, K.F., Miao, X.D., et al. 2025. Holocene extreme flood distribution patterns in the upper and middle Yellow River: A review based on slackwater deposits. Earth-Science Reviews, 261, 105039.

Garcin, Y., Schefuß, E., Schwab, V.F., Garreta, V., Gleixner, G., Vincens, A., Todou, G., Sen e, O., Onana, J.-M., Achoundong, G., Sachse, D., 2014. Reconstructing C 3 and C4 vegetation cover using n-alkane carbon isotope ratios in recent lake sediments from Cameroon, Western Central Africa. Geochem. Cosmochim. Acta

https://doi.org/10.5194/egusphere-2026-4480
Preprint. Discussion started: 4 September 2026

142, 482e500. https://doi.org/10.1016/j.gca.2014.07.004.

He, H.M., Zhang, Q.F., Zhou, J., et al. Coupling climate change with hydrological dynamic in Qinling Mountains, China. Climatic Change. DOI 10.1007/s10584-008-9527-5.

Hosner D, Wagner M, Tarasov P E, et al. 2016. Spatiotemporal distribution patterns of archaeological sites in China during the Neolithic and Bronze Age: An overview. The Holocene, 26(10), 1576-1593.

Inglis, G.N., Farnsworth, A., Lunt, D., et al., 2015. Descent toward the Icehouse: Eocene Sea surface cooling inferred from GDGT distributions. Paleoceanography. 29 https:// doi.org/10.1002/2014PA002723.

Koutavas, A., Joanides, S., 2012. El Nino-Southern ˜ Oscillation estrama in the Holocene and last glacial maximum. Plaeoceanography 27, PA4208.

Lacoul, P., Freedman, B., 2006. Environmental influences on aquatic plants in freshwater ecosystems. Environ. Rev. 14, 89e136. https://doi.org/10.1139/a06- 00.

Leipe, C., Long, T. W., Sergusheva, E. A., Wagner, M., and Tarasov, P. E. 2019. Discontinuous spread of millet agriculture in eastern Asia and prehistoric population dynamics, Sci. Adv., 5, eaax6225, https://doi.org/10.1126/sciadv.aax6225

Li Y.N., Gu, Y.S., Jiang, M.J., et al. 2025. Neolithic human adaptations to the environmental changes in the Jianghan Plain, middle Yangtze Valley. Quaternary Science Reviews, 355, 109271.

Li, H.B., Zhang, Y.Y., Feng, Z.D., 2023b. Precipitation variations since the last Deglacial reconstructed from pollen records in the central Plains of China. Quat. Int. 669, 1–11. https://doi.org/10.1016/j.quaint.2023.05.018.

Li, M.Y., Jia,W., Yang, Y., et al. 2026. Spatial patterns of Asian summer monsoon precipitation in the Chinese monsoon region since the LGM. npj | climate and atmospheric science, 9-27. https://doi.org/10.1038/s41612-026-01345-4.

Li, Q., Wu, H.B., Cheng, J., et al. 2024. Hydroclimatic changes in eastern China during the Holocene based on pollen data and climate modeling. Global and Planetary Change, 234,104391.

https://doi.org/10.5194/egusphere-2026-4480
Preprint. Discussion started: 4 September 2026

Li, X.F., Wang, N.L., Wu, Z.H. 2021. Terrain Effects on Regional Precipitation in a Warm Season over Qinling-Daba Mountains in Central China. 12, 1685. https://doi.org/10.3390/atmos12121685.

Li, X.Q., Shang, X., Dodson, J., et al. 2009. Holocene agriculture in the Guanzhong Basin in NW China indicated by pollen and charcoal evidence. The Holocene, 19, 8, 1213–1220.

Lin, D., Zhang, E., Liu, E., Sun, W., Wang, R., Meng, X., Ni, Z., Wang, Y., You, Y., 2024. Human impacts overwhelmed climate as the dominant factor controlling lacustrine organic matter accumulation in Erhai Lake 2000 years ago, Southwest China. Sci. Total Environ. 946, 174182.

Liu, C., Hui, Z.C., Zhang, Y.Y. et al. 2025. Holocene precipitation reconstruction in the Central Plains of China: Evidence from a high-resolution pollen record. Catena, 261, 109588.

Liu, H.Y., Gu, Y.S., Huang, X.Y., Yu, Z.C., Xie, S.C., Cheng, S.G., 2019. A 13000 years peatland palaeohydrological response to the ENSO-related asian monsoon precipitation changes in the middle Yangtze Valley. Quat. Sci. Rev. 212, 80–91. https://doi.org/10.1016/j.quascirev.2019.03.034.

Liu, J., Shen, Z., Chen, W., Chen, J., Zhang, X., Chen, J., Chen, F., 2020a. Dipolar mode of precipitation changes between north China and the Yangtze River Valley existed over the entire Holocene: evidence from the sediment record of Nanyi Lake. Int. J. Climatol. 41 (3), 1667–1681.

Liu, X.X., Sun, Y.B., Vandenberghe, J., Cheng, P., Zhang, X., Gowan, E.J., Lohmann, G., An, Z.S., 2020b. Centennial- to millennial-scale monsoon changes since the last deglaciation linked to solar activities and North Atlantic cooling. Clim. Past. 16, 315–324.

Nichols, J.E., Walcott, M., Bradley, R.s., Pilcher, J., Huang, Y.S., 2009. Quantitative assessment of precipitation seasonality and summer surface wetness using ombrotrophic sediments from an Arctic Norwegian peatland. Quat. Res. 72, 443e451.

Pei, Z.Q., Wang, J., Li, Y.X., Liu, C.C., Quan, Y.B., Li, H.M., Yang, Y.S., Cheng, T., Yi,

https://doi.org/10.5194/egusphere-2026-4480
Preprint. Discussion started: 4 September 2026

M.J., Zhang, L., Wang, H., Xia, H., Chen, F.H., Zhang, D.J.. 2026. Reassessing the Neolithic Chronology and Cultural Development at the Dadiwan Site. Science China Earth Sciences, doi: 10.1007/s11430-025-1928-4.

Rao, Z., Li, Y., Zhang, J., Jia, G., Chen, F., 2016. Investigating the long-term palaeoclimatic controls on the δD and δ18O of precipitation during the Holocene in the Indian and East Asian monsoonal regions. Earth Sci. Rev. 159, 292–305.

Reimer, P.J., Austin, W.E.N., Bard, E., et al. 2020. The IntCal20 Northern Hemisphere radiocarbon age calibration curve (0-55 cal kBP). Radiocarbon, 62, 725-757. https://doi.org/10.1017/RDC.2020.41.

Shen, J., Zhang, E.L., Zhang, Z.L., et al. 2000. A preliminary study on forming age of the Nansihu Lake. J. Lake Sci. 12, 91–93. https://doi.org/10.18307/2000.0114 (in Chinese).

Sun, A.Z., Feng, Z.D., 2013. Holocene climatic reconstructions from the fossil pollen record at Qigai Nuur in the southern Mongolian Plateau. Holocene 23 (10), 1391–1402. https://doi.org/10.1177/0959683613489581.

Sun, W., Zhang, E., Liu, E., You, Y., Li, J., Ni, Z., Meng, X., Zhang, W., Chen, R., 2023. Hydroclimate changes since the last glacial maximum from sedimentary biomarkers in a crater lake in the Great Khingan Mountains. Northeast China. Quat. Sci. Rev. 312, 108175.

Tian, L.N., Yan, B.P., He, C.G., et al. Paleolakes in the lower Yellow River plain since the last deglaciation: age, distribution, and mechanism. Catena, 259, 109315.

Xiao, Q.L., D. Wu, W. Sun et al., Recurring dipole flooding patterns in East Asia throughout the Holocene, Science Bulletin, https://doi.org/10.1016/j.scib.2026.01.052.

Xu, Q.H., Xiao, J.L., Li, Y.C., Tian, F., Nakagawa, T., 2010. Pollen-based quantitative reconstruction of Holocene climate changes in the Daihai lake area, inner mongolia. China. J. Clim. 23 (11), 2856–2868. https://doi.org/10.1175/2009JCL13155.1.

Zhang, C., Zhao, C., Zhou, A., Zhang, K., Wang, R., Shen, J., 2019. Late Holocene lacustrine environmental and ecological changes caused by anthropogenic

https://doi.org/10.5194/egusphere-2026-4480
Preprint. Discussion started: 4 September 2026

activities in the Chinese Loess Plateau. Quat. Sci. Rev. 203, 266–277.

Zhang, J.H., Guan, Y.J., Xin, Y.H., et al., 2024. The spatiotemporal distribution and environmental suitability evaluation of Neolithic settlements in the Western Guanzhong Basin of China. The Holocene, 1–13.

Zhang, J.N., Xia, Z.K. 2011. Deposition Evidences of the 4 ka BP Flood Events in Central China Plains. ACTA GEOGRAPHICA SINICA, 66, 5. (In Chinese with English abstract).

Zhang J P, Huan X J, Lü H Y, et al. 2022. Crossing of the Hu line by Neolithic population in response to seesaw precipitation changes in China. Sci Bull, 67(8), 844-852. https://doi.org/10.1016/j.scib.2021.12.011

Zhang, Y., Cui, Q.Y., Liang, Chen, et al. 2025. Quantitative pollen reconstruction of temperature and precipitation in the subtropical-temperate climate transition zone of East-Central China since the Last Glacial Maximum. Quaternary Science Reviews, 367, 109528.

Zhang, Z.K., Wang, S.M., Shen, J., et al., 1999. River channel changes recorded by Lake sediments in Nansihu Lake, the lower reaches of the Yellow River. J. Lake Sci. 11, 231-236 (in Chinese).

Zhao, Q.K., Peng, YX., Wang, M.T., 2013. Environment Change and Cultural Response in Holocene in South Shandong.

Zhu, Z.M., Feinberg, J.M., Xie, S.C., Bourne, M.D., Huang, C.J., Hu, C.Y., Chen, H., 2017. Holocene ENSO-related cyclic storms recorded by magnetic minerals in speleothems of central China. Proc. Natl. Acad. Sci. 114 (5), 852–857. https://doi.org/10.1073/pnas.1610930114.

Zou, C.H., Zhao, Q., M, L.J. 2020. Holocene environmental evolution recorded by core sediments of Judian Lake in the east of Lubei Plain, Shandong Province. Journal of Palaeogeography, 22, 6. (In Chinese with English abstract).

https://doi.org/10.5194/egusphere-2026-4480
Preprint. Discussion started: 4 September 2026

Figures

Figure.1 Location of key sites mentioned in the text (a and b):Nansi Lake (NS; this study), Qigai Nuur Lake (QGN; Sun and Feng, 2013), Daihai Lake (Xu et al., 2010), Gonghai Lake (Chen et al., 2015), Ansai Loess (ASL; Gao et al., 2019), Dadiwan Loess (DDWL; Liu et al., 2020), Baoji Loess (BJL; Beck et al., 2018), Mianchi Basin (MC; Li et al., 2023), Xingying Basin (XY; Liu et al., 2025), Dajiuhu Peat (DJH; Liu et al., 2019), Heshang Cave (HS; Zhu et al., 2017), Jianghan Plain (JH; Li et al., 2025), Nanyi Lake (NY; Liu et al., 2021). (c) Mean monthly temperature and precipitation at the Jining meteorological station, Shandong Province, China. Data are sourced from the China Meteorological Administration.

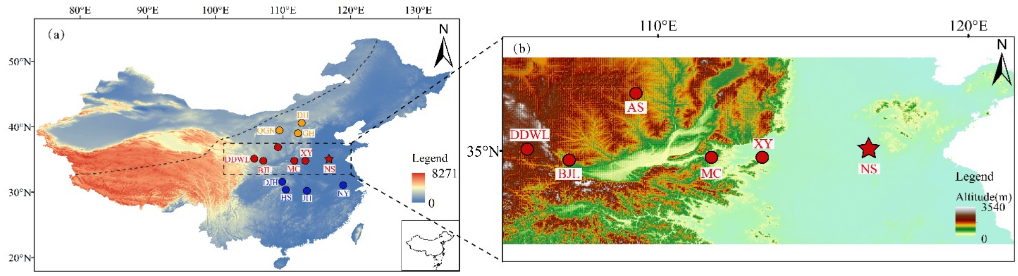

https://doi.org/10.5194/egusphere-2026-4480
Preprint. Discussion started: 4 September 2026

581 Figure. 2 Choronlogy and lithology of the sediment core from Nansi Lake. (a) Core
582 photograph showing overall sediment characteristics. (b) Lithology profile illustrating
583 stratigraphic changes along the core. (c) Age–depth model based on calibrated AMS
584 ^{14}C dates and Bayesian modeling using the Bacon age-modelling software. (d) 210Pb
585 and 137Cs activities (Bq/kg) of dried sedements.

586 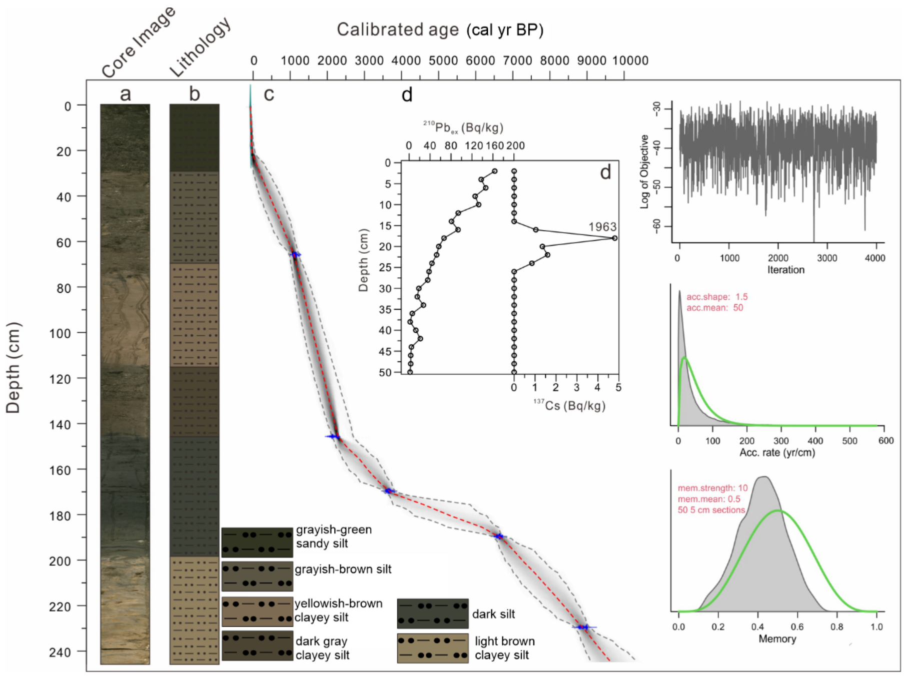

https://doi.org/10.5194/egusphere-2026-4480
Preprint. Discussion started: 4 September 2026

Figure. 3 Average molecular distribution of n-alkanes and teporal variraitons in n-alkanes proxies in sediments from Nansi Lake. Average relative abundances of odd-carbon n-alkanes in different age intervals: (a) <2500 cal yr BP, (b) 2500-6000 cal yr BP, (c)>6000 cal yr BP, (d) the average of the whole core. Error bars represent the standard deviation of samples within each interval. Down-core variations in n-alkanes proxies during the Holocene: (e) Paq, reflecting the relative contribution of submerged/floating aquatic macrophytes to sedimentary organic matter; (f) C_{23}/C_{31}, representing the relative contribution of aquatic macrophyte-derived mid-chain n-alkanes versus terrestrial higher-plant-derived long-chain n-alkanes; and (g) LPTP, indicating the ratio of lake productivity/terrigenous organic production.

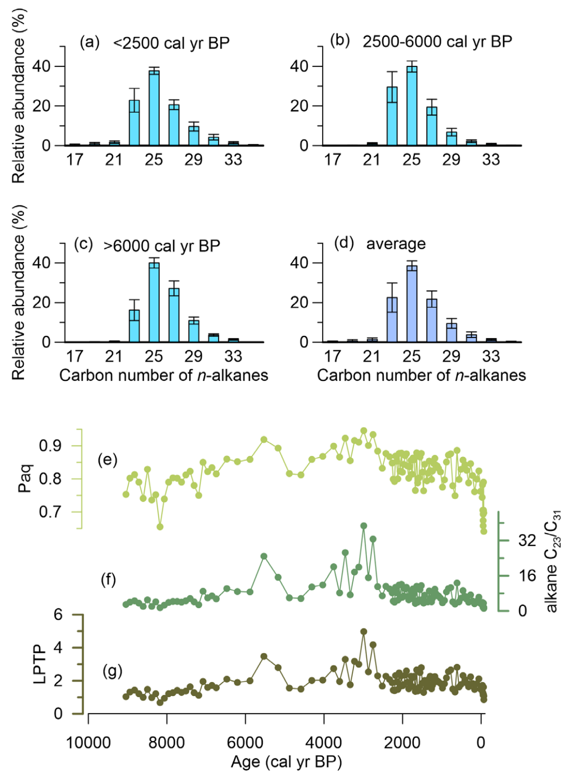

https://doi.org/10.5194/egusphere-2026-4480
Preprint. Discussion started: 4 September 2026

Figure. 4 Comparison of various hydroclimate record from transition region of EAM and other Holocene moisture records from northern and central China. (a) Precipitation at Daihai Lake (Xu et al., 2010). (b) Precipitation at Qigai Nuur (Sun and Feng, 2013). (c) Precipitation at Gonghai Lake (Chen et al., 2015). (d) Lake water depth at Nansi Lake (this study). (e) Precipitation at Baoji Loess (Beck et al., 2018). (f) Hydrological conditions at Heshang (Zhu et al., 2017). (g) Depth to water table at Dajiu Peat (Liu et al., 2019). (h) Hydrological conditions at Jianghan Plain (Li et al., 2025). (i) Nanyi Lake (Liu et al., 2021).

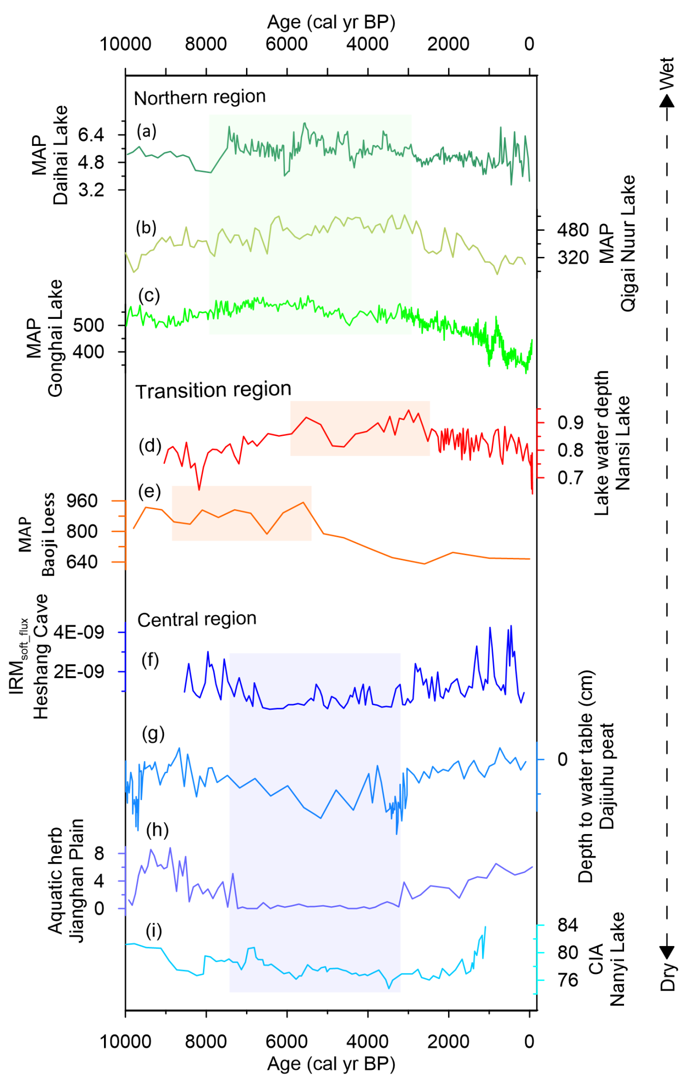

https://doi.org/10.5194/egusphere-2026-4480
Preprint. Discussion started: 4 September 2026

Figure.5 Comparison of various hydroclimate record from transition region of EAM. (a) Large flood record at the western and central of transition zone (Xiao et al., 2026). (b) Precipitation at Mianchi Basin (Li et al., 2023) and Xingying Basin (Liu et al., 2025). (c) Precipitation and moisture records at Ansai Loess (Gao et al., 2019), Dadiwan Loess (Liu et al., 2020), Baoji Loess (Beck et al., 2018). (d) Large flood record at the estern of transition zone (Xiao et al., 2026). (e) Lake water depth at Nansi Lake (this study), probability density function for lacustrine occurrences (Tian et al., 2025). (f) El Niño activity record from foraminiferal $\delta^{18}O$ at eastern equatorial Pacific.

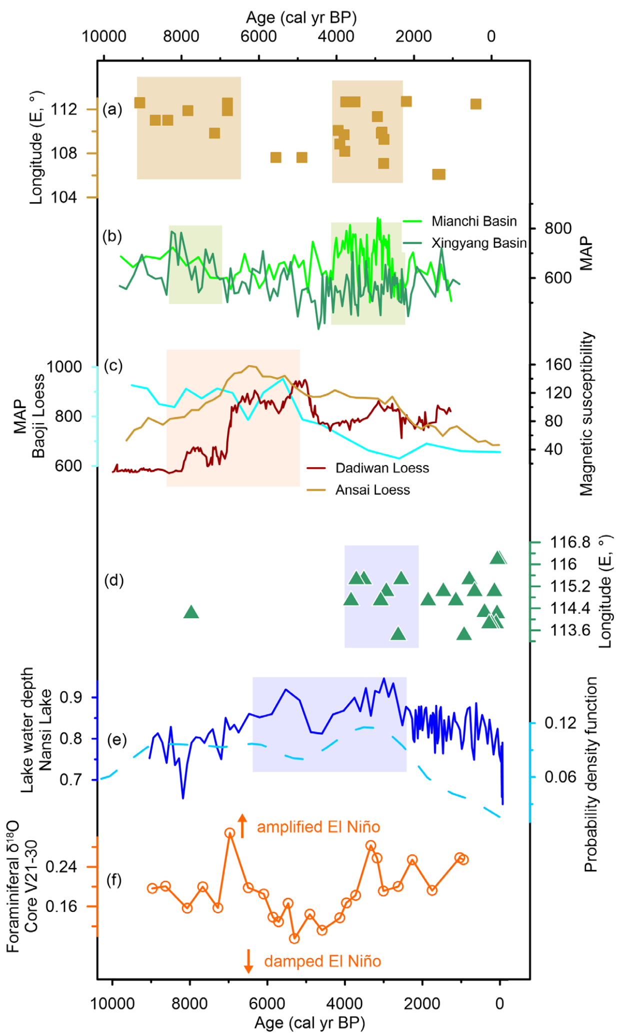

https://doi.org/10.5194/egusphere-2026-4480
Preprint. Discussion started: 4 September 2026

Figure. 6 Patterns of rainfall departure for summer (JJA) (mm) averaged for (a) 1951–1978 and (b) 1979–1992.

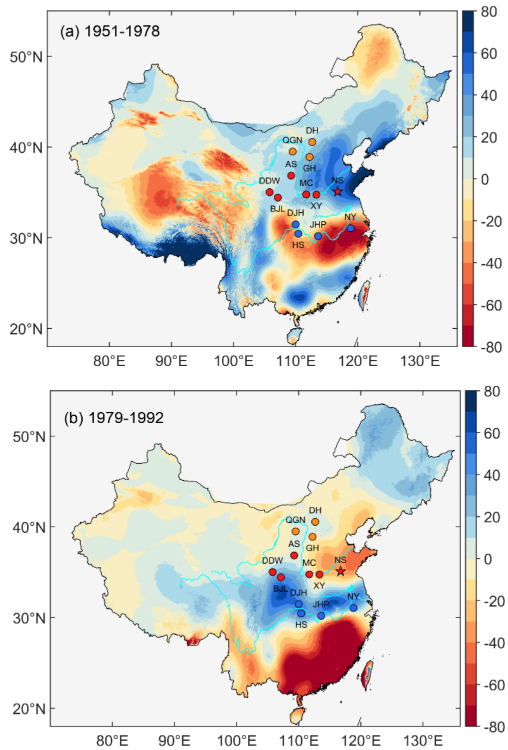

https://doi.org/10.5194/egusphere-2026-4480
Preprint. Discussion started: 4 September 2026

Figure. 7 Spatiotemporal changes in archaeological site density across the East Asian summer monsoon transition zone. Kernel density estimation (KDE) maps of archaeological sites are shown for six 1000-year intervals: (A) 8000–7000 cal yr BP, (B) 7000–6000 cal yr BP, (C) 6000–5000 cal yr BP, (D) 5000–4000 cal yr BP, (E) 4000–3000 cal yr BP, and (F) 3000–2000 cal yr BP. Archaeological site data were extracted from Hosner et al. (2016). Black dots represent archaeological sites in each time interval, and the color scale indicates relative KDE intensity, with warmer colors denoting higher site density.